RSC Advances

PAPER

View Article Online
View Journal | View Issue

Cite this: *RSC Adv.*, 2018, **8**, 17034

Effects of area, aspect ratio and orientation of rectangular nanohole on the tensile strength of defective graphene – a molecular dynamics study

Xinmao Qin, *[a] Wanjun Yan,[a] Xiaotian Guo [b] and Tinghong Gao[c]

Molecular dynamics simulations with adaptive intermolecular reactive empirical bond order (AIREBO) potential are performed to investigate the effects of rectangular nanoholes with different areas, aspect ratios (length/width ratios) and orientations on the tensile strength of defective graphene. The simulations reveal that variation of area, aspect ratio and orientation of rectangular nanohole can significantly affect the tensile strength of defective graphene. For example, defective graphene with a larger area of rectangular nanohole shows a bigger drop in tensile strength. It was found that the tensile strength of both armchair and zigzag edged graphene monotonically decreases with area increases in rectangular nanohole. Changes in aspect ratio and orientation of rectangular nanohole, however, can either decrease or increase the tensile strength of defective graphene, dependent on the tensile direction. This study also presents information that the tensile strength of defective graphene with large area of nanohole is more sensitive to changes in aspect ratio and orientation than is defective graphene with small area of nanohole. Interestingly, variation of tensile strength of defective graphene from MD simulations is in good agreement with predictions from energy-based quantized fracture mechanics (QFM). The present results suggest that the effect of nanoholes on the tensile strength of graphene provides essential information for predictive optimization of mechanical properties and controllable structural modification of graphene through defect engineering.

Received 19th March 2018
Accepted 24th April 2018

DOI: 10.1039/c8ra02415d

rsc.li/rsc-advances

1. Introduction

Graphene is a two-dimensional single atomic layer material, which consists of carbon atoms packed in a honeycomb structure.[1] Its extraordinary geometric and electronic structure afford graphene excellent physical, chemical and mechanical properties,[2–5] such as high carrier mobility, large specific surface area, high fracture intrinsic strength and elastic modulus. Such properties make graphene suitable for applications in various fields, for example, in nanocomposites,[6] chemical sensors,[7] supercapacitors,[8] lithium-ion batteries,[9] DNA-sequencing tools[10] and selective molecular sieving devices.[11] However, the inadvertent introduction of various topological defects (vacancy, substitutional atom, adatom, Stone–Thrower–Wales defect, dislocation and grain boundary) and other large-sized defects (nanopore, nanocrack and nanohole) is unavoidable in the process of preparation and manipulation of graphene-based devices.[12] In addition, such defects can also occur as a result of the conditions in which graphene-based devices are used,[13] and previous study has shown that structural defects in a graphene sheet have great influence on its properties.[14,15] For example, a vacancy defect can significantly decrease the fracture strength and Young's modulus of graphene sheet, and the Young's modulus stabilization after reconstruction of the vacancy defect.[16,17] The Young's modulus of a nitrogen-doped graphene sheet is independent of the concentration of nitrogen, but silicon-doped graphene shows a notable weakening in its Young's modulus.[18] The tensile strength of graphene decreases markedly with increase in the number of substitutional nitrogen and silicon atoms, and then the fracture behavior of graphene transforms from ductile to brittle.[13,19] Pei[20] and co-workers found that adsorption of hydrogen on a graphene sheet can drastically deteriorate its Young's modulus, failure strength and fracture strain. They further investigated the mechanical properties of methyl (CH_3) functionalized graphene, and found that these are dependent on the position, distribution and coverage of CH_3 radicals on graphene.[21] The effects of Stone–Thrower–Wales (STW) defect, grain boundaries (GBs) and dislocation on the mechanical properties of the graphene sheet were researched based on molecular dynamics simulations. Different types of STW defect have different effects on the mechanical properties of graphene sheet.[22,23] When there is more than one STW defect, the fracture strength of graphene is affected by the orientation of the multiple defects.[24]

[a]*School of Electronic and Information Engineering, Anshun University, Anshun, 561000, China. E-mail: qxm200711@126.com*

[b]*School of Mathematics and Physics, Anshun University, Anshun, 561000, China*

[c]*College of Big Data and Information Engineering, Guizhou University, Guiyang, 550025, China*

Successful preparation of polycrystalline graphene is necessary to study the relationships between the structure of grain boundaries of polycrystalline graphene and its mechanical properties. Wei[25] and Han[26] reported that grain boundary defects can either increase or decrease the fracture strength of graphene, dependent on the specific arrangement of the defects, not just their concentration. Meng[27] *et al.* presented a comprehensive study of the dependency between the nanocrack and dislocation in graphene sheet, identifying that dislocation in graphene will shield the process of nanocrack propagation. Except for the topological defects, the influence of large sized defects (nanopore, nanocrack) on graphene sheet has been explored. After studying the mechanical properties of graphene with various shapes, sizes and density of nanopore, Liu[28] and David[29] concluded that the tensile strength of graphene decreases with increasing size and density of nanopore. Zhang[30] and Zhao[31] found that the fracture strength of graphene declines as the length of nanocrack increases, and Le and Batra[32–35] further reported the effects of crack length on the crack propagation rate and the fracture behavior.

In summary, the appearance of defects in graphene can weaken its mechanical properties, such as fracture strength, Young's modulus and fracture strain. However, such defects have potential in novel applications of graphene, for example, as molecule capacitors and nanofilters. Unfortunately, there are very few studies on the effects of large sized rectangular nanoholes with different characteristics on the mechanical properties of graphene, and such study is necessary for further applied research of graphene-based nanocomposites and nanosensors.

In the current study, molecular dynamics simulations were performed using LAMMPS (Large-scale Atomic/Molecular Massively Parallel Simulator)[36,37] with the adaptive intermolecular reactive empirical bond order (AIREBO) potential. Systematic investigations were made into the effects of rectangular nanoholes of various areas, aspect ratios (length/width ratio) and orientations on the tensile strength of defective graphene. It was found that the tensile strength of both armchair and zigzag edged graphene monotonically decreases with area increases of nanohole. With changes of aspect ratio and orientation of rectangular nanohole, however, the defect can either decrease or increase the tensile strength of defective graphene, dependent on the tensile direction. It is also suggested that the tensile strength of defective graphene with large area of nanohole is more sensitive to changes in aspect ratio and orientation than is defective graphene with small area of nanohole. The current findings will provide a useful guideline for designing mechanically robust graphene-enhanced nanocomposites and graphene-based devices, such as nanosensors, DNA-sequencing tools and selective molecular sieving devices.

2. Simulation conditions and methods

2.1 Initial conditions

The tensile model of the graphene sheet consisted of 3807 carbon atoms, with zigzag and armchair edges of 10 nm. The center of the graphene sheet was located at the origin of the coordinate system, and the zigzag and armchair edges were parallel to the x and y directions, respectively. This means that the process of loading in the $x(y)$ direction is the tensile deformation along the zigzag (armchair) graphene sheet (Fig. 1(a) and (b)). By deleting specified carbon atoms at the centered region of the graphene sheet, models of rectangular nanohole with different areas, aspect ratios and orientations were created. In the simulation, the areas of rectangular nanohole are 1 nm^2, 2 nm^2, 4 nm^2 and 6 nm^2, respectively. a/b is defined as the aspect ratio of rectangular nanohole, and the aspect ratio of rectangular nanohole is equal to 2 : 1, 3 : 1 and 4 : 1, respectively. The orientation of the nanohole is further defined as the tilting angle (θ), and this angle is between the direction of the "a" axis of rectangular nanohole and the zigzag direction of the graphene sheet (Fig. 1). When $\theta = 0°$, the "a" axis of nanohole parallels the zigzag direction (Fig. 1(c) and (d)), when $\theta = 90°$, the

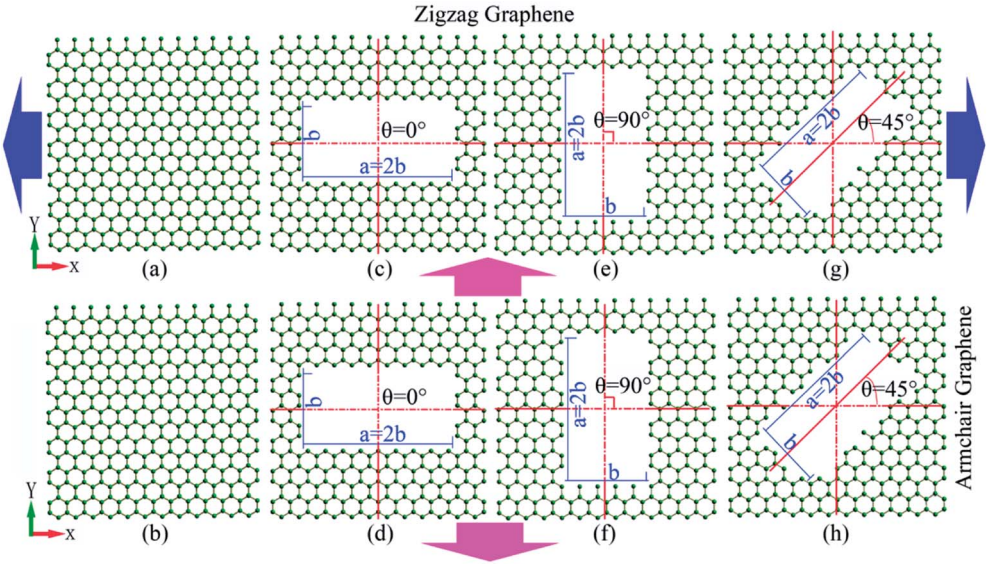

Fig. 1 Models of tensile deformation of pristine graphene or defective graphene with rectangular nanohole.

"*a*" axis is perpendicular to the zigzag direction of the graphene sheet (Fig. 1(e) and (f)).

Periodic boundary conditions were applied in all directions. Using the steepest descent algorithm, energy minimization configurations of the system were performed by iteratively adjusting the coordinates of the carbon atoms of the graphene. Prior to tensile deformation, the tensile model was relaxed at 300 K and 0 bar pressure through an isothermal–isobaric ensemble (NPT) for 10 ps. All the tensile deformations of graphene are carried out at a constant temperature of 300 K, which was realized using a Nose–Hoover thermostat.[38–41] Uniaxial tensile loading with a strain rate of 0.005 ps^{-1} was applied to the x or y directions of graphene, with simulation timestep of 0.001 ps. To analyze the behavior of fracture of defective graphene, the atomic configuration was visualized and the stress distributions of carbon atoms were determined using OVITO[42] (The Open Visualization Tool), an open source visualization tool for molecular dynamics simulation. The tensile strength of defective graphene is defined as the point at which the maximum stress is reached. To obtain the stress–strain curve, the thickness of the graphene sheet was first defined as 3.4 Å.

2.2 Potential between atoms

The C–C interatomic interactions in graphene were calculated using adaptive intermolecular reactive empirical bond order (AIREBO) potential,[36] which has been extensively used to simulate the mechanical properties of graphene. This potential enables the breaking and creation of covalent bonds, and has been successfully applied in studies of the properties of carbon-based nanomaterials.[37] The AIREBO potential consists of three terms:

$$E = \frac{1}{2}\sum_{i}\sum_{j\neq i}\left[E_{ij}^{\mathrm{REBO}} + E_{ij}^{\mathrm{LJ}} + \sum_{k\neq i,j}\sum_{l\neq i,j,k} E_{kijl}^{\mathrm{TORSION}}\right] \quad (1)$$

the E_{ij}^{REBO} gives the model its reactive capabilities and describes only short-ranged C–C interactions (r < 2 angstroms), the E_{ij}^{LJ} term adds longer-ranged interactions (2 < r < cutoff), and the $E_{kijl}^{\mathrm{TORSION}}$ term is an explicit 4-body potential that describes various dihedral angle preferences in hydrocarbon configurations.

3. Results and discussions

To search for reasonable strain rate of the graphene sheet, tensile deformations with various loading rates were performed using the LAMMPS package. Fig. 2 shows variation of tensile strength (zigzag direction, armchair direction, the average strength of the zigzag and armchair directions) of pristine graphene with strain rate from 5×10^{-5} ps^{-1} to 5×10^{-2} ps^{-1}. From Fig. 2, it can be concluded that the tensile strength increases with the strain rate. As the strain rate ranges from 5×10^{-5} ps^{-1} to 5×10^{-2} ps^{-1}, the strength gap between zigzag and armchair graphene gets smaller and smaller. When the strain rate is 1×10^{-2} ps^{-1} (and 5×10^{-2} ps^{-1}), the strength of zigzag graphene is almost equal to that of armchair graphene. Fig. 2 also shows the comparison of tensile strength (zigzag direction, armchair direction, the averaged strength among the zigzag and armchair direction) between the present work and results from the study described in ref. 23 (with temperature and strain rate of tensile deformation being 300 K and 5×10^{-3} ps^{-1}, respectively). Thus, the tensile strength of the present research is in accordance with the results from ref. 23. Consequently, the strain rate of 5×10^{-3} ps^{-1} was applied in the present tensile deformation.

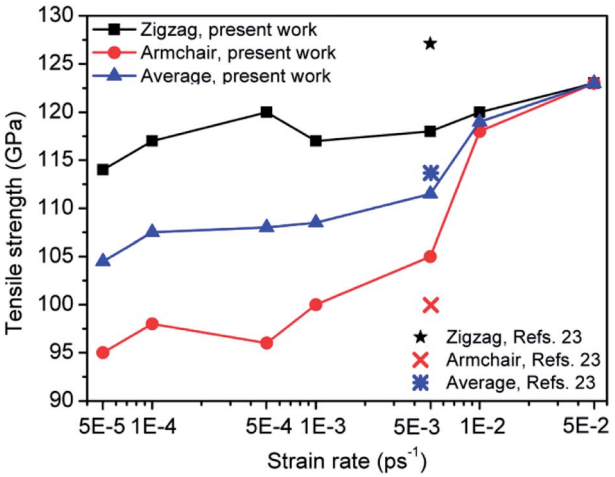

Fig. 2 Effects of strain rate on tensile strength of pristine graphene in the present work, and the comparison of tensile strength between the present work and ref. 23 (strain rate of 5×10^{-3} ps^{-1}).

To further validate the proposed computational method and model, a comparison of mechanical properties between the present study (strain rate of 5×10^{-3} ps^{-1} and temperature of 300 K) and those from the literature is shown in Table 1. The calculated tensile strengths of pristine zigzag and armchair graphene are about 118 GPa and 105 GPa, respectively. The

Table 1 Comparison of mechanical properties of pristine graphene between the present results and those from the literature

	E_{average} (TPa)	$\sigma_{\mathrm{average}}$ (GPa)	σ_{zig} (GPa)	σ_{arm} (GPa)	$\varepsilon_{\mathrm{zig}}$	$\varepsilon_{\mathrm{arm}}$
Experiment[3]	1.0	123.5	—	—	—	—
DFT[4]	—	—	121	110	0.266	0.194
MD & orthogonal tight-binding (TB) method (300 K)[5]	1.03 ± 0.03	115.5	129	102	0.2	0.13
MD (300 K)[20]	0.86	121	137	105	0.27	0.17
MD (300 K)[23]	—	113	126	100	0.22	0.13
MD (0 K)[35]	1.04	118.5	126	111	0.238	0.191
Present work (300 K)	0.83	114	118	105	0.32	0.24

computed Young's modulus and tensile strength, averaged among the zigzag and armchair graphene sheet, are 0.83 TPa and 114 GPa, respectively, and the tensile strains of zigzag and armchair graphene sheet are 0.32 and 0.24, respectively. There is no large difference between the present results and those from the literature.[3–5,20,23,35]

3.1 Effects of area of rectangular nanohole on the tensile strength of graphene sheet

To study the effects of the areas of nanohole on the tensile strength of graphene sheet, defective graphene—with rectangular nanohole of four area types—was loaded in the zigzag and armchair directions, respectively. Fig. 3 shows the stress–strain curves of pristine graphene and defective graphene with areas of 1 nm^2, 2 nm^2, 4 nm^2 and 6 nm^2 nanohole (with aspect ratio and tilting angle of nanohole maintained at 2 : 1 and 0°, respectively). The tensile strength of defective graphene decreases with increasing area of nanohole.

To understand the mechanism of fracture of the defective graphene, snapshots of the tensile deformation process of graphene with the area of 2 nm^2 nanohole are shown in Fig. 4 (with aspect ratio and tilting angle of nanohole maintained at 2 : 1 and 0°, respectively). The von Mises stress of the graphene is calculated, and the stress distribution is plotted by the color contour in the figures. At the beginning of the tensile deformation, the stress of carbon atoms is maintained at a relatively low level (Fig. 4(a) and (e)). With increasing tensile deformation (the Fig. 4(b) and 4(f)), the atomic stress is considerably increased, and there is obvious stress concentration present at the local region of defective graphene (Fig. 4(b), the up and down red region of defective graphene; Fig. 4(f), the left and right red region of defective graphene). There is then nanocrack formation and gradual growth at the local high-stress region (Fig. 4(c), the left-up position; Fig. 4(g), the right-middle position). Subsequently, fracture of the defective graphene sheet occurs at the local region of stress concentration (Fig. 4(d) and (h)). From Fig. 4, the regions of stress concentrations of defective graphene were located at the up and down region of defective graphene for the zigzag deformation (or at the left and right region for the armchair deformation). The region of stress concentration, termed the "effective loading area" (the red region in Fig. 4), clearly affected the tensile strength of defective graphene.

3.2 Effect of aspect ratio of rectangular nanohole on the tensile strength of graphene sheet

Fig. 5 shows the dependence of tensile strength of defective graphene on the aspect ratio of rectangular nanohole at different areas and tilting angles. When the tilting angle of rectangular nanohole is 0° (the orange and deep skyblue insets in Fig. 5(a) and (b)), no matter the area of nanohole, the tensile strength of zigzag (armchair) defective graphene sheet increases (decreases) with aspect ratio from 2 : 1 to 3 : 1 to 4 : 1 (Fig. 5(a) and (b)). For different areas of rectangular nanohole, with the increasing aspect ratio, the variation in tensile strength is similar. From Fig. 5(c) and (d), it can be seen that the slope of tensile strength *versus* aspect ratio curves changes with tilting angle of rectangular nanohole (with the area of nanohole maintained at 6 nm^2). When the tilting angle is 0°, the strength of zigzag (armchair) defective graphene relatively increases (decreases); but as the tilting angle moves to 60°, the strength of zigzag (armchair) defective graphene slightly decreases (increases); finally, when the tilting angle is 90°, the variations of strength of defective graphene with aspect ratio of rectangular nanohole become obvious (the tensile strength of zigzag and armchair defective graphene become small and large, respectively). Comparing the variation tendency of tensile strength (the curves of Fig. 5) and the tensile model (the insets of Fig. 5) of defective graphene sheet, it was found that the tensile strength increases as the aspect ratio increases, with the direction of the long axis ("*a*" axis in Fig. 1) of rectangular nanohole parallel to the tensile direction of defective graphene sheet (the orange insets in Fig. 5). For the direction of the long axis of rectangular nanohole perpendicular to the tensile direction of defective graphene sheet, however, the tensile strength decreases as the aspect ratio increases (the deep skyblue insets in Fig. 5).

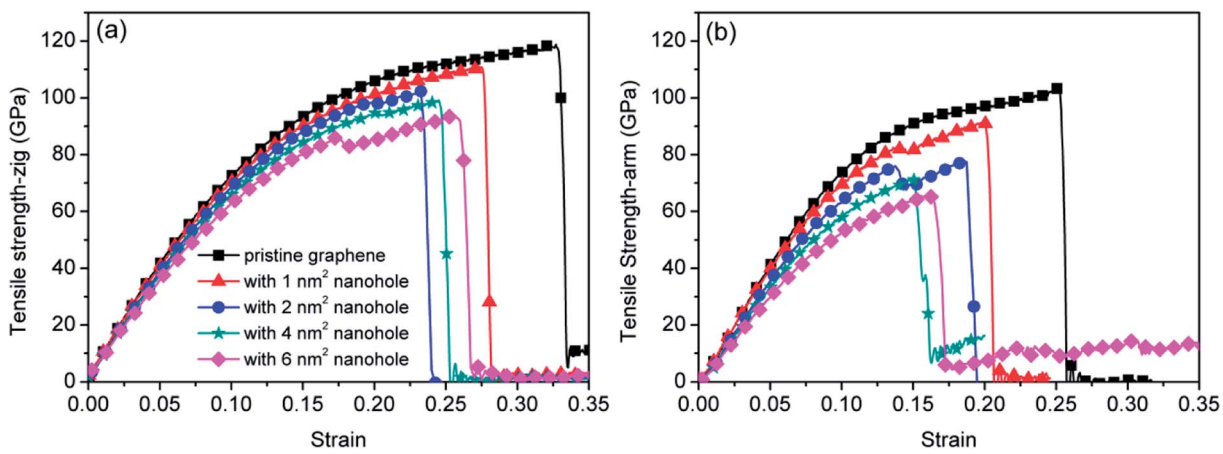

Fig. 3 Stress–strain curves of pristine graphene and defective graphene with different areas of rectangular nanohole (at constant aspect ratio of 2 : 1 and tilting angle of 0°). (a) and (b) show loading along the zigzag and armchair directions, respectively.

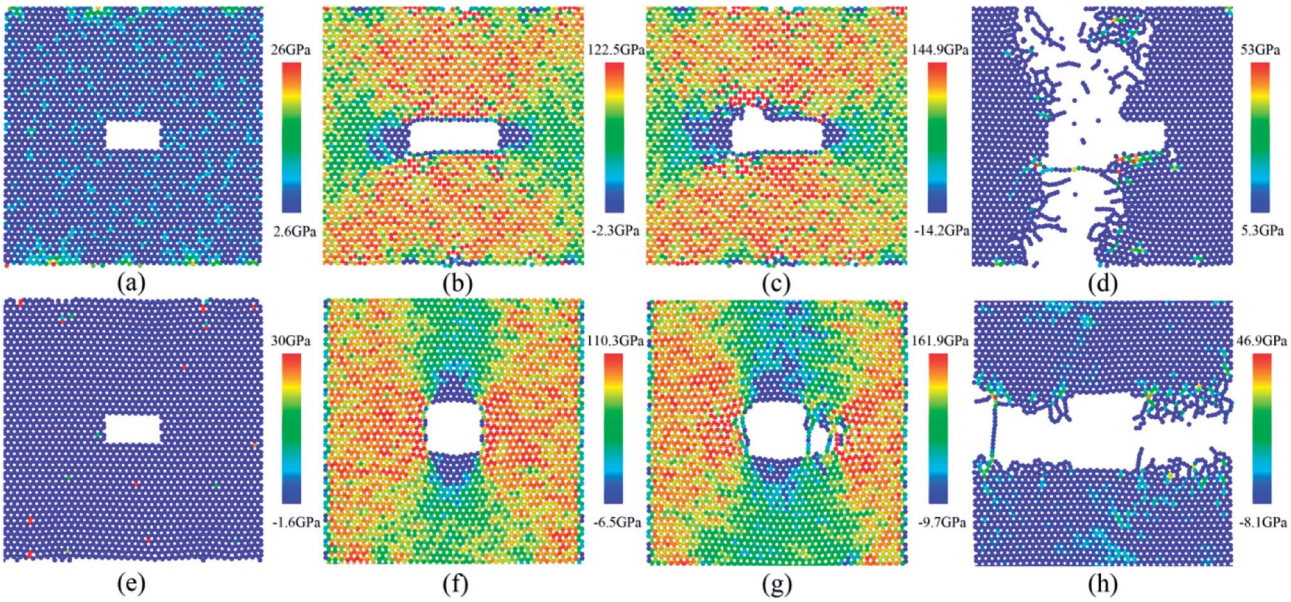

Fig. 4 Snapshots of the tensile deformation process of defective graphene sheet with the area of 2 nm^2 rectangular nanohole for aspect ratio of 2 : 1 and tilting angle of 0°. (a)–(d) and (e)–(h) denote the zigzag and armchair tensile deformation processes, respectively. (a) and (e) von Mises stress distribution at the start of tensile deformation. (b) and (f) Stress distribution before the nanocrack formation. (c) and (g) Nanocrack formation and growth. (d) and (h) Fracture of defective graphene sheet. The color bar represents the magnitude of stress of carbon atoms in the graphene.

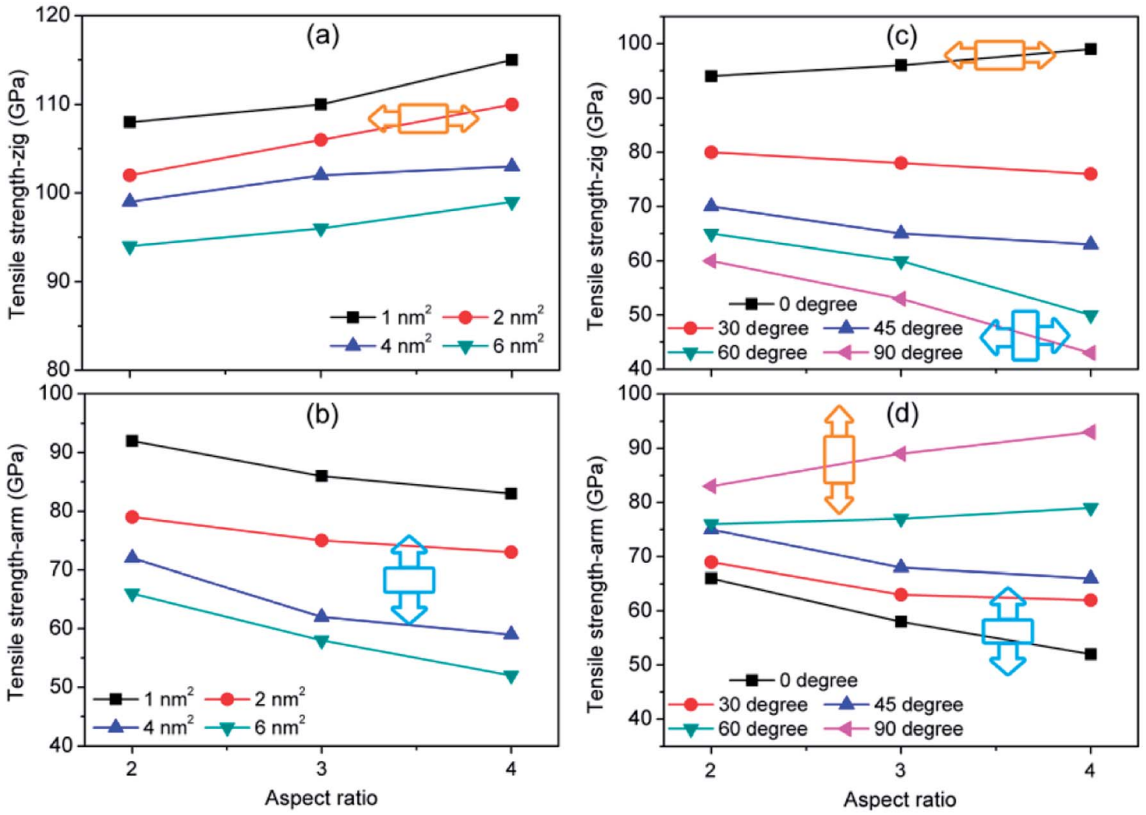

Fig. 5 Dependence of the tensile strength of defective graphene on the aspect ratio of rectangular nanohole at different areas ((a) and (b)) and tilting angles ((c) and (d)). The insets show the tensile model of defective graphene sheet with rectangular nanohole (tilting angle of 0° and 90°), the rectangle and arrow denote the rectangular nanohole and tensile direction, respectively. (a), (c) and (b), (d) show loading along the zigzag and armchair directions, respectively.

3.3 Effect of tilting angle of rectangular nanohole on the tensile strength of graphene sheet

Fig. 6 shows the effect of tilting angle of rectangular nanohole (with different aspect ratios and areas) on the tensile strength of defective graphene sheets. No matter the variation of aspect ratio and area of rectangular nanohole, the tensile strength of zigzag defective graphene decreases, but the strength of armchair defective graphene increases with increasing tilting angle of rectangular nanohole.

In Fig. 6(a) and (b), when the area of rectangular nanohole is maintained at 6 nm^2, but the tilting angle is varied from 0° to 90°, the degree of weakening (strengthening) of tensile strength for zigzag (armchair) graphene sheet is dependent on the aspect ratio of the rectangular nanohole. For an aspect ratio of 2 : 1, the tensile strength of zigzag (armchair) defective graphene slowly decreases (increases) with increasing tilting angle. But with an aspect ratio of 4 : 1, with increasing tilting angle, the zigzag and armchair defective graphene undergo a process of significant weakening and strengthening, respectively.

From Fig. 6(c) and (d), for different areas of nanohole, there are dramatic changes in degree of tensile strength of defective graphene with increases in the tilting angle of the nanohole (with aspect ratio maintained at 4 : 1). For example, when the area of nanohole in the graphene sheet is 1 nm^2, the strengths of zigzag defective graphene with nanohole of tilting angles of 0°, 30°, 45°, 60° and 90° are 115 GPa, 98 GPa, 94 GPa, 92 GPa and 99 GPa, respectively (with tensile strength of zigzag pristine graphene sheet of 118 GPa). The strengths of armchair graphene with nanohole of tilting angles of 0°, 30°, 45°, 60° and 90° are 83 GPa, 89 GPa, 84 GPa, 87 GPa and 97 GPa, respectively (with tensile strength of armchair pristine graphene of 105 GPa). There is a minor change in the tensile strength with tilting angle increases (area of rectangular nanohole with 1 nm^2), but when the area of nanohole is more than 1 nm^2, such as at 2 nm^2, 4 nm^2 and 6 nm^2, the tensile strength of zigzag (armchair) defective graphene is monotonically decreased (increased) along with the tilting angle of nanohole from 0° to 90°. During the tensile deformation of defective graphene with area of nanohole 2 nm^2, the tensile strength of zigzag (armchair) defective graphene is gently decreased (increased) with increasing tilting angle. When the area of nanohole is up to 6 nm^2, however, the zigzag (armchair) defective graphene undergoes a process of sharp weakening (strengthening). It can be summarized that variation in tilting angle of rectangular nanohole can cause decrease or increase in tensile strength of the graphene sheet. In addition, when the area and aspect ratio of the rectangular nanohole are large, the weakening or strengthening effects of rectangular nanohole on the tensile strength of defective graphene are considerably more.

4. Discussions

In the tensile deformation process of pristine graphene, the stress on each carbon atom is gradually and uniformly increased with increasing tensile strain until fracture. When

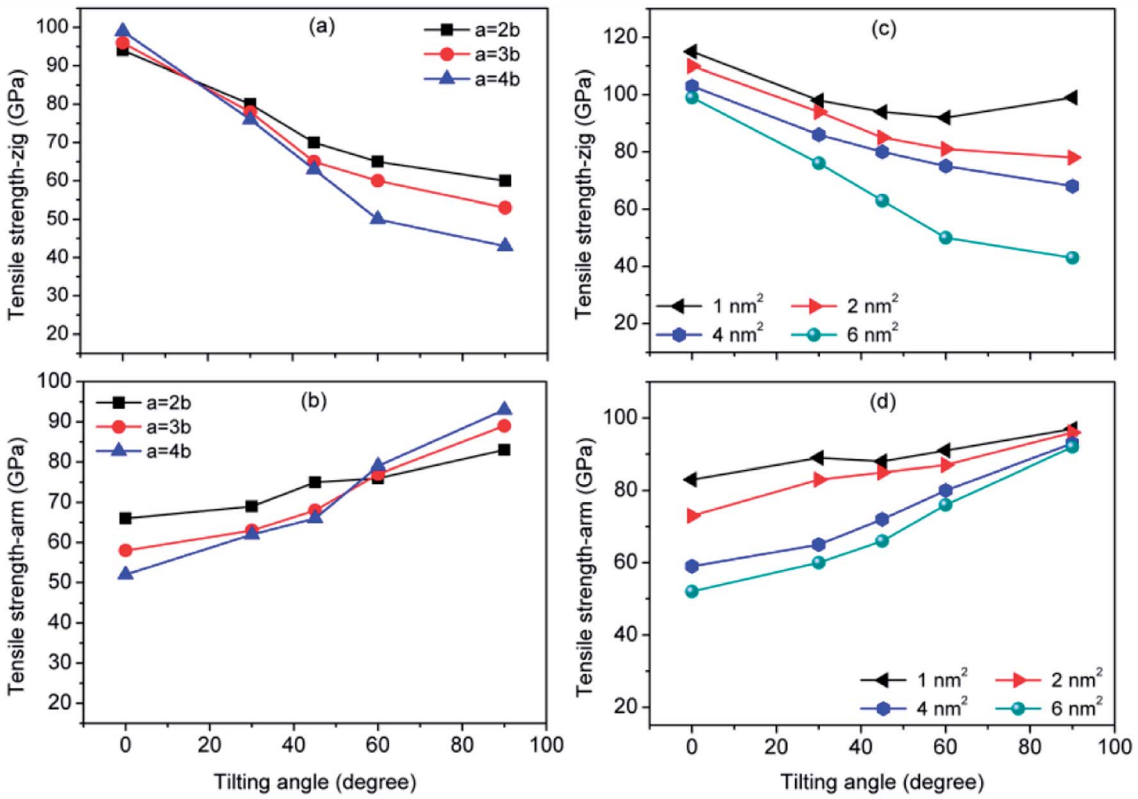

Fig. 6 Dependence of the tensile strength of defective graphene sheet on the tilting angle of rectangular nanohole at different aspect ratio ((a) and (b)) and area ((c) and (d)). (a), (b) and (c), (d) are loaded along the zigzag and armchair directions, respectively.

tensile deformation of graphene with rectangular nanohole is performed, however, the imperfect structure of defective graphene results in uneven distributions of stress on the carbon atoms. This is because the rectangular nanohole disrupts the perfect structure of the graphene, reducing the effective loading area of graphene during the tensile deformation. Therefore, the tensile strength of defective graphene sheet will be decreased, and as the area of rectangular nanohole increases, the tensile strength of defective graphene becomes smaller and smaller.

Similar results were obtained from quantized fracture mechanics (QFM), an energy-based theory based on discrete crack growth, proposed by substituting the differentials in Griffith's energy balance equation with finite differences.[23,31,43,44] QFM can be applied to study the tensile strength of defective graphene with defects of any size and shape. Under the I loading, a blunt nanocrack (length is $2L$) on finite-width graphene (width is 2ω) is considered in this study. The tensile strength of graphene with nanohole σ_f using QFM is given by[31,43,44]

$$\sigma_f(L) = \sigma_r(\dot{\varepsilon}, T)\sqrt{\frac{1+\frac{\rho}{2L_0}}{1+\frac{2L}{L_0}}\left[\frac{2\omega}{\pi L}\tan\left(\frac{\pi L}{2\omega}\right)\right]^{\frac{1}{2}}} \quad (2)$$

where the σ_r is the ideal tensile strength of pristine zigzag (armchair) graphene sheet. $\rho = \frac{\sqrt{3}}{2}L_0$ is the tip radius of the nanocrack in the graphene, and $L_0 = \sqrt{3}r_0$ is the fracture quantum, which is defined as the minimum nanocrack extension corresponding to the breaking of one interatomic bond perpendicular to the tensile direction ($r_0 = 1.42$ Å is the carbon–carbon bond length in graphene sheet).[31] In prediction of tensile strength of defective graphene with rectangular nanohole using QFM, it must be pointed out that the nanocrack length $2L$ of formula (2) corresponds to the length of the void perpendicular to the tensile direction in defective graphene sheet. Fig. 7 shows a comparison of tensile strength of defective graphene between the molecular dynamics simulations (MD) and quantized fracture mechanics (QFM). From Fig. 7(a), the tensile strength of graphene (both zigzag and armchair direction) from MD and QFM both decreased with increasing area of rectangular nanohole. The strength of defective graphene from MD is larger than that from QFM, perhaps because the shape of nanohole in the present simulations is a rectangle, but not a perfectly sharp rectangular nanohole.

From Fig. 7(b), increasing aspect ratio of rectangular nanohole (from 2 : 1 to 4 : 1) can strengthen (weaken) the defective zigzag (armchair) graphene both from MD simulations and QFM predictions. When the tilting angle of the rectangular nanohole is increased from 0° to 90°, the variations in defective graphene from the MD calculations correspond well with the tendency from QFM theoretical prediction, as shown in Fig. 7(c). This change in tensile strength of defective graphene occurs mainly because the rectangular nanohole of effective length perpendicular to the tensile direction changes with increasing aspect ratio and tilting angle of rectangular nanohole (Fig. 8). And the effective loading area of the defective graphene sheet will also change. For example, when the

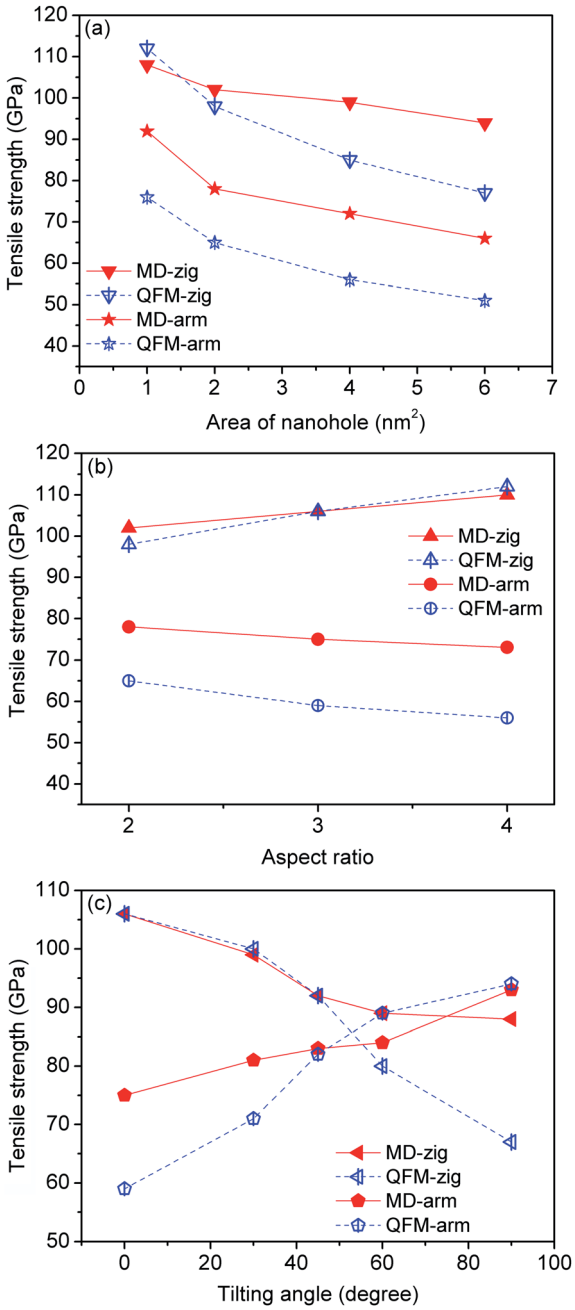

Fig. 7 Comparison of tensile strength of graphene sheet between molecular dynamics simulations (MD) and quantized fracture mechanics (QFM). The red points and blue points denote the tensile strength from MD and QFM, respectively. (a), (b) and (c) indicate strength variations of graphene sheet with increases of area, aspect ratio and tilting angle of rectangular nanohole, respectively.

area and tilting angle are kept constant but the aspect ratio of the rectangular nanohole is increased from 2 : 1 to 4 : 1, the effective length of the rectangular nanohole of zigzag (armchair) graphene sheet becomes small (large), but the effective loading area of zigzag (armchair) graphene sheet becomes large (small). When the area and aspect ratio are kept constant but the tilting angle of the rectangular nanohole is increased from 0° to 90°, the effective loading areas of zigzag and armchair graphene sheet become small and large, respectively. This variation of effective loading

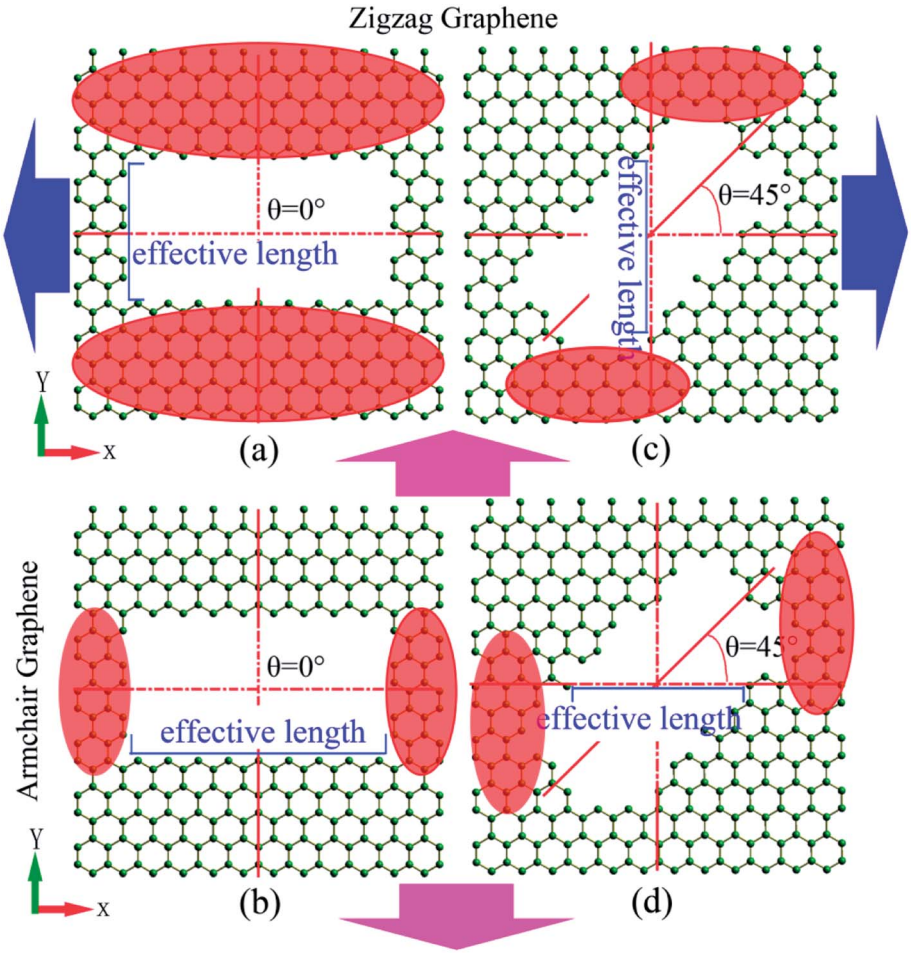

Fig. 8 Variations of effective length of rectangular nanohole and the effective loading area of defective graphene sheet with increase in tilting angle of rectangular nanohole. The region of red ellipsoid denotes the effective loading area of defective graphene sheet.

area of defective graphene ultimately results in the regular change of tensile strength of defective graphene sheet.

5. Conclusions

In this study, the effects of areas, aspect ratios and orientations of rectangular nanohole were studied on the tensile strength of graphene sheet using molecular dynamics simulations based on the adaptive intermolecular reactive empirical bond order (AIREBO) potential. It was found that the tensile strength of defective graphene sheet significantly relied on the area, aspect ratio and orientation of rectangular nanohole. With increasing area of rectangular nanohole, both the tensile strength of zigzag and armchair graphene sheet monotonically decrease. In addition, the aspect ratio and orientation of rectangular nanohole also have influence on the tensile strength of defective graphene. When the long axis ("*a*" axis) of rectangular nanohole is parallel to the tensile direction, the tensile strength of defective graphene increases with the aspect ratio increase. But for the condition of the long axis of nanohole perpendicular to the tensile direction, the tensile strength of graphene decreases with the aspect ratio increase. Moreover, when the tilting angle of rectangular nanohole ranges from 0° to 90°, the tensile strength of defective zigzag graphene gradually drops, but the tensile strength of defective armchair graphene increases. Furthermore, it was found that the tensile strength of defective graphene is more sensitive to the tilting angle of nanohole at larger area and aspect ratio than at smaller area and aspect ratio. Comparing the effects of area, aspect ratio and orientation on the tensile strength of defective graphene, it can be concluded that the tensile strength of graphene with rectangular nanohole mainly depends on the rectangular nanohole of size perpendicular to the tensile direction, named for the effective nanocrack length. For instance, when the area of nanohole is kept constant, the tensile strength of defective graphene decreases with increase in effective nanocrack length. The variation of tensile strength of MD simulations is in good agreement with that predicted by the energy-based quantized fracture mechanics (QFM). The present results suggest that the effect of rectangular nanohole on the tensile strength of graphene provides essential information for predictive optimization of mechanical properties and controllable structural modification of graphene through topological defect engineering. And the findings will also provide a useful guideline for designing mechanically robust graphene-enhanced nanocomposites and graphene-based devices, such as nanosensors, DNA-sequencing tools and selective molecular sieving devices.

Conflicts of interest

There are no conflicts to declare.

Acknowledgements

This work is supported by the Natural Science Foundation of Guizhou Province of China (Grant No. [2015]2001), the innovation team of Anshun University (Grant No. 2015PT02), and the school project of Anshun University (Grant No. [2015]AQ07).

References

1 A. K. Geim and K. S. Novoselov, The rise of graphene, *Nat. Mater.*, 2007, **6**(3), 183–191.
2 K. S. Novoselov, Z. Jiang, Y. Zhang, S. V. Morozov, H. L. Stormer, U. Zeitler, J. C. Maan, G. S. Boebinger, P. Kim and A. K. Geim, Room-temperature quantum hall effect in graphene, *Science*, 2007, **315**(5817), 1379.
3 C. Lee, X. Wei, J. W. Kysar, *et al.*, Measurement of the Elastic Properties and Intrinsic Strength of Monolayer Graphene, *Science*, 2008, **321**, 385–388.
4 F. Liu, P. Ming and J. Li, Ab initio calculation of ideal strength and phonon instability of graphene under tension, *Phys. Rev. B: Condens. Matter Mater. Phys.*, 2007, **76**, 064120.
5 H. Zhao, K. Min and N. R. Aluru, Size and chirality dependent elastic properties of graphene nanoribbons under uniaxial tension, *Nano Lett.*, 2009, **9**(8), 3012–3015.
6 Y. Teng Liang, B. K. Vijayan, K. A. Gray, *et al.*, Minimizing graphene defects enhances Titania nanocomposite-based photocatalytic reduction of CO_2 for improved solar fuel production, *Nano Lett.*, 2011, **11**(7), 2865–2870.
7 Y.-H. Zhang, Ya-B. Chen, K.-G. Zhou, *et al.*, Improving gas sensing properties of graphene by introducing dopants and defects: a first-principles study, *Nanotechnology*, 2009, **20**, 185504.
8 C. Liu, Z. Yu, D. Neff, *et al.*, Graphene-based supercapacitor with an ultrahigh energy density, *Nano Lett.*, 2010, **10**(12), 4863–4868.
9 Z.-S. Wu, W. Ren, L. Xu, *et al.*, Doped graphene sheets as anode materials with superhigh rate and large capacity for lithium ion batteries, *ACS Nano*, 2011, **5**(7), 5463–5471.
10 S. J. Heerema and C. Dekker, Graphene nanodevices for DNA sequencing, *Nat. Nanotechnol.*, 2016, **11**, 127–136.
11 S. P. Koenig, L. Wang, J. Pellegrino, *et al.*, Selective molecular sieving through porous graphene, *Nat. Nanotechnol.*, 2012, **7**, 728–732.
12 R. Khare, S. L. Mielke, J. T. Paci, *et al.*, Coupled quantum mechanical/molecular mechanical modeling of the fracture of defective carbon nanotubes and graphene sheets, *Phys. Rev. B*, 2007, **75**, 075412.
13 A. Zandiatashbar, G.-H. Lee, S. Joo An, *et al.*, Effect of defects on the intrinsic strength and stiffness of graphene, *Nat. Commun.*, 2014, **5**, 3186.
14 F. Banhart, J. Kotakoski and A. V. Krasheninnikov, Structural defects in graphene, *ACS Nano*, 2011, **5**(1), 26–41.
15 W. Yan, Q. Xie, X. Qin, *et al.*, First-principle analysis of photolelectronic properties of silicon-carbon materials with graphene-like honeycomb structure, *Comput. Mater. Sci.*, 2017, **126**, 336–343.
16 N. Jing, Q. Xue, C. Ling, *et al.*, Effect of defects on Young's modulus of graphene sheet: a molecular dynamics simulation, *RSC Adv.*, 2012, **2**, 9124–9129.
17 H. Tongwei, H. Pengfei, W. Jian, *et al.*, Effect of Vacancy Defects on Tensile Mechanical Properties of Single Graphene Sheets, *Journal of Tongji University (Natural Science)*, 2010, **38**(8), 1210–1214.
18 Z. Xiaoxi, L. Junhua, L. Xuyang, *et al.*, Influence of silicon doping on mechanical properties of graphene sheets under tension, *Journal of University of Science and Technology of China*, 2014, **44**(3), 238–243.
19 B. Mortazavi, S. Ahzi, V. Toniazzo, *et al.*, Nitrogen doping and vacancy effects on the mechanical properties of graphene: A molecular dynamics simulation, *Phys. Lett. A*, 2012, **376**, 1146–1153.
20 Q. X. Pei, Y. W. Zhang and V. B. Shenoy, A molecular dynamics study of the mechanical properties of hydrogen functional graphene, *Carbon*, 2010, **48**, 898–904.
21 Q.-X. Pei, Y.-W. Zhang and V. B. Shenoy, Mechanical properties of methyl functionalized graphene: a molecular dynamics simulation, *Nanotechnology*, 2010, **21**, 115709.
22 T. Han, Y. Shi, P. He, *et al.*, The effect of Stone-Wales topological defects on the tensile mechanical properties of single graphene sheets, *Chin. J. Solid Mech.*, 2011, **32**(6), 619–624.
23 M. C. Wang, C. Yan, L. Ma, *et al.*, Effect of defects on fracture strength of graphene sheets, *Comput. Mater. Sci.*, 2012, **54**, 236–239.
24 L. He, S. Guo, J. Lei, *et al.*, The effect of Stone-Thrower-Wales defects on mechanical properties of graphene sheets – A molecular dynamics study, *Carbon*, 2014, **75**, 124–132.
25 Y. Wei, J. Wu, H. Yin, *et al.*, The nature of strength enhancement and weakening by pentagon-heptagon defect in graphene, *Nat. Mater.*, 2012, **11**, 759–763.
26 J. Han, S. Ryu, D. Sohn, *et al.*, Mechanical strength characteristics of asymmetric tilt grain boundaries in graphene, *Carbon*, 2014, **68**, 250–257.
27 F. Meng, C. Chen, J. Song, *et al.*, Dislocation shielding of a nanocrack in graphene: Atomistic simulation and Continuum modeling, *J. Phys. Chem. Lett.*, 2015, **6**(20), 4038–4042.
28 Y. Liu and X. Chen, Mechanical properties of nanoporous graphene membrane, *J. Appl. Phys.*, 2014, **115**, 034303.
29 D. Cohen-tanugi and J. C. Grossman, Mechanical strength of nanoporous graphene as a desalination membrane, *Nano Lett.*, 2014, **14**(11), 6171–6178.
30 B. Zhang, L. Mei and H. Xiao, Nanofracture in graphene under complex mechanical stresses, *Appl. Phys. Lett.*, 2012, **101**, 121915.
31 H. Zhao and N. R. Aluru, Temperature and strain-rate dependent fracture strength of graphene, *J. Appl. Phys.*, 2010, **108**, 064321.

32 M.-Q. Le and R. C. Batra, Single-edge crack growth in graphene sheets under tension, *Comput. Mater. Sci.*, 2013, **69**, 381–388.
33 M.-Q. Le and R. C. Batra, Crack propagation in pre-strained single layer graphene sheets, *Comput. Mater. Sci.*, 2014, **84**, 238–243.
34 M.-Q. Le and R. C. Batra, Mode-I stress intensity factor in single layer graphene sheets, *Comput. Mater. Sci.*, 2016, **118**, 251–258.
35 M.-Q. Le, Y. Umeno, Fracture of monolayer boronitrene and its interface with graphene, *Int. J. Fract.*, 2017, **205**(2):151–168.
36 S. J. Stuart, A. B. Tutein and J. A. Harrison, A Reactive Potential for Hydrocarbons with Intermolecular Interactions, *J. Chem. Phys.*, 2000, **112**, 6472–6486.
37 B. Ni, S. B. Sinnott, P. T. Mikulski, *et al.*, Compression of carbon nanotubes filled with C_{60}, CH_4, or Ne: predictions from molecular dynamics simulations, *Phys. Rev. Lett.*, 2002, **88**, 205505.
38 G. J. Martyna, D. J. Tobias and M. L. Klein, Constant pressure molecular dynamics algorithms, *J. Chem. Phys.*, 1994, **101**, 4177–4189.
39 M. Parrinello and A. Rahman, Polymorphic transitions in single crystals : A new molecular dynamics method, *J. Appl. Phys.*, 1981, **52**(12), 7182–7190.
40 M. E. Tuckerman, J. Alejandre, R. López-Rendón, *et al.*, A Liouville-operator derived measure-preserving integrator for molecular dynamics simulations in the isothermal–isobaric ensemble, *J. Phys. A: Math. Gen.*, 2006, **39**, 5629–5651.
41 W. Shinoda, M. Shiga and M. Mikami, Rapid estimation of elastic constants by molecular dynamics simulation under constant stress, *Phys. Rev. B*, 2004, **69**, 134103.
42 A. Stukowski, Visualization and analysis of atomistic simulation data with OVITO – the open Visualization Tool, *Modell. Simul. Mater. Sci. Eng.*, 2010, **18**, 015012.
43 N. Pugno, A. Carpinteri, M. Ippolito, *et al.*, Atomistic fracture : QFM *vs.* MD, *Eng. Fract. Mech.*, 2008, **75**, 1794–1803.
44 N. M. Pugno and R. S. Ruoff, Quantized fracture mechanics, *Philos. Mag.*, 2004, **84**(27), 2829–2845.